Compact 0.7 mJ/11 ns eye-safe erbium laser

2016 Laser Phys. 26 125801

(http://iopscience.iop.org/1555-6611/26/12/125801)

IOP Publishing | Astro Ltd Laser Physics

Laser Phys. **26** (2016) 125801 (6pp) doi:10.1088/1054-660X/26/12/125801

Compact 0.7 mJ/11 ns eye-safe erbium laser

V V Vitkin[1], V M Polyakov[1], A A Kharitonov[1], V A Buchenkov[2], A Yu Rodionov[2], A A Zhilin[3], O S Dymshits[3] and P A Loiko[4]

[1] ITMO University, 49 Kronverkskiy pr., 197101 Saint-Petersburg, Russia
[2] Vavilov State Optical Institute, 5, kor. 2 Kadetskaya liniya V.O., 199053 Saint-Petersburg, Russia
[3] NITIOM S.I. Vavilov State Optical Institute, 36 Babushkina St., 192171 Saint-Petersburg, Russia
[4] Center for Optical Materials and Technologies (COMT), Belarusian National Technical University, 65/17 Nezavisimosti Ave., 220013 Minsk, Belarus

E-mail: v.v.v@bk.ru

Received 26 August 2016, revised 10 October 2016
Accepted for publication 18 October 2016
Published 16 November 2016

Abstract

We report on the development of a compact diode-end-pumped eye-safe (~1.54 μm) passively-cooled Er,Yb:glass laser. The design of this laser is facilitated by the use of a double-pass pumping scheme and a special ZrO_2 diffuse reflector for a uniform pump distribution. In the free-running mode, this laser generates 8.2 mJ/3 ms pulses with a slope efficiency of 15%. Passive Q-switching is provided by saturable absorbers made of transparent glass-ceramics containing Co^{2+}:γ-Ga_2O_3 or Co^{2+}:$MgAl_2O_4$ nanocrystals with a spinel structure. In the latter case, 0.7 mJ/10.5 ns pulses are generated corresponding to >60 kW peak power and good beam quality ($M^2 = 1.4$). The designed laser is suitable for portable range-finders.

Keywords: erbium laser, Q-switching, cobalt, spinel, glass-ceramics, eye-safe

(Some figures may appear in colour only in the online journal)

1. Introduction

There is a growing interest for eye-safe laser sources emitting at ~1.5 μm [1]. This radiation is strongly absorbed by the eye's cornea and lens and thus it cannot reach the sensitive retina. In addition, the ~1.5 μm wavelength corresponds to the transparency window of the atmosphere that is useful for free-space applications. Typically, such emission is provided by lasers based on erbium (Er^{3+}) ions and operating on the $^4I_{13/2} \rightarrow {}^4I_{15/2}$ transition. Er lasers have found their recognized applications in free-space optical communication, remote sensing (LIDAR technology), wind sensing and range-finding [2–7] in civil and military fields. The requirements for range-finders operating at low pulse frequencies include a high pulse energy and peak power, good beam quality and low divergence, as well as a compact and robust design, preferentially with passive cooling of a laser head [7–10].

State-of-the-art materials for compact Er lasers are phosphate glasses codoped with Er^{3+} and Yb^{3+} ions [11]. Codoping with Yb^{3+} ions is needed to provide the efficient pumping of the laser material at 960–980 nm according to the $^2F_{7/2} \rightarrow {}^2F_{5/2}$ transition of the Yb^{3+} ions. This spectral range corresponds to emission wavelengths of the cost-effective commercial high-power InGaAs laser diodes. The excitation of the Er^{3+} ions is then provided by the $Yb^{3+} \rightarrow Er^{3+}$ energy-transfer (ET). Commercial phosphate glasses provide long storage times of the Er^{3+} ions ($\tau(^4I_{13/2})$ ~8 ms) and high ET efficiency ($\eta_{ET} > 98\%$) [11, 12]. Glasses are produced by a standard melt-quenching method that provides size-scalable production of laser elements with a high optical quality—a strong advantage over the single-crystal technology. The single drawback of the glasses is their poor thermal conductivity and low thermal fracture limit [12]. Significant attention should be paid to the elimination of heat and uniform pumping of an Er glass laser element, which contradicts the requirement of passive cooling. Thus, the designing of compact cost effective passively-cooled and efficient Er laser oscillators is a complicated and very demanding task.

The generation of a pulsed output from a compact Er laser is normally provided by the passive Q-switching (PQS) due to the introduction of a proper saturable absorber (SA) into the laser cavity. In this way, pulses with the duration of a few tens of ns and pulse energies of a few mJ can be achieved. The well-recognized SAs for an Er laser are based on cobalt (Co^{2+}) ions located in tetrahedral sites of crystals, e.g. Co^{2+}:$MgAl_2O_4$ single crystal (Co^{2+}:spinel) [13].

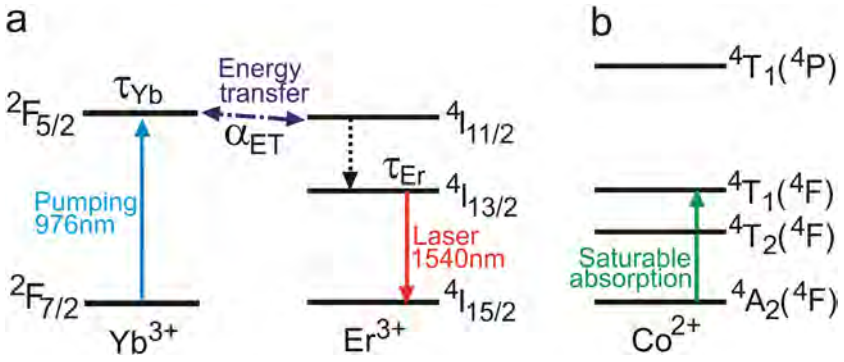

Figure 1. Simplified scheme of energy levels of (a) Yb^{3+} and Er^{3+} ions and (b) Co^{2+} ions in tetrahedral (T_d) sites.

Recently, transparent glass-ceramics (GCs) containing various Co^{2+}-doped nanocrystals, e.g. $MgAl_2O_4$ [14], $ZnAl_2O_4$ [15], γ-Ga_2O_3 [16], and ZnO [17], have been studied for the replacement of single crystalline SAs. The GCs are synthesized by a cost-effective melt-quenching method with subsequent heat-treatments and possess good optical homogeneity [14, 15]. The nonlinear properties and laser-induced damage threshold (LIDT) for GCs are comparable or even advantageous with respect to the Co^{2+}:$MgAl_2O_4$ single crystals [14–16].

In the present paper, we report on the design of a compact and efficient passively-cooled eye-safe laser oscillator based on the Er,Yb:glass and GC SA capable of generating ~1 mJ pulses corresponding to the peak power of >60 kW at ~1.54 μm.

2. Modeling gain in the active element

At first, we used a simple rate equation model to describe the gain characteristics of a Er,Yb:glass laser element. This modeling was used to optimize the element length and duration of the pump pulses in order to reach a simultaneously compact design and maximum single-pass gain. The model is as follows. The Er^{3+}, Yb^{3+}-codoped glass laser rod is longitudinally end-pumped by an InGaAs laser diode at 976 nm. The pumping is performed at a low repetition rate (1 Hz) and the duration of a single pump pulse is about a few ms. The simplified scheme of the energy levels of Er^{3+} and Yb^{3+} ions is shown in figure 1 and the corresponding system of the rate equations is [10]:

$$\frac{\partial N_{Yb}}{\partial t} = W_p(x,y,z,t) - \frac{N_{Yb}}{\tau_{Yb}} - \alpha_{ET} N_{Yb}(N_{Er}^0 - N_{Er}), \qquad (1a)$$

$$\frac{\partial N_{Er}}{\partial t} = \alpha_{ET} N_{Yb}(N_{Er}^0 - N_{Er}) - \frac{N_{Er}}{\tau_{Er}}. \qquad (1b)$$

Here, N_{Yb} and N_{Er} are the population densities of the Yb^{3+} and Er^{3+} ions in the $^2F_{5/2}$ and $^4I_{13/2}$ multiplets, respectively, which are the functions of coordinates (x, y, z) and time t, N_{Er}^0 is the doping concentration of the Er^{3+} ions, τ_{Yb} and τ_{Er} are the lifetimes of the above mentioned states of the Yb^{3+} and Er^{3+} ions, respectively, α_{ET} is the microscopic ET parameter, $W_p(x, y, z, t)$ is the pump rate, $W_p = P'_{abs}/h\nu_p$ where P'_{abs} is the volumetric density of the absorbed pump power, h is the Planck constant, and ν_p is the pump frequency. The system of the rate equations does not take into account upconverison and excited-state absorption [10, 18]; the non-radiative relaxation from the $^4I_{13/2}$ state to the lower-lying multiplet is considered as a single depopulation channel for this state. The parameters used for the calculation are listed in table 1.

The Er,Yb:glass rod is considered to have the following dimensions: diameter: 1 mm, length: 10 mm. The rod is pumped at 976 nm by a diode located at 0.5 mm from the input face. The emitting area of the diode is 0.4 × 0.4 mm^2 and the beam divergence is 4°. The optical power of the diode is 10 W. We used a beam tracing algorithm to calculate the pump rate $W_p(x, y, z, t)$ and considered the rectangular temporal profile of the pump pulses. The bleaching of the Yb^{3+} absorption was taken into account.

After solving the system of the rate equations numerically, we have derived the integral single-pass gain $g(x, y, z, t)$ at each point of the rod:

$$g(x,y,z,t) = \int_0^z k_g(x,y,z',t)\mathrm{d}z', \qquad (2a)$$

$$k_g = N_{Er}\sigma_{SE}^L - (N_{Er}^0 - N_{Er})\sigma_{abs}^L. \qquad (2b)$$

where k_g is the gain coefficient, σ_{SE}^L and σ_{abs}^L are the stimulated-emission and absorption cross-sections of the Er^{3+} ions at the laser frequency ν_L. The distribution of g in the cross-section of a 10 mm-long laser rod at different moments after the pump turn-on is shown in figure 2(a). The dependence of g on the rod length and the duration of pump pulses is presented in figure 2(b). From these figures, for the design of an Er,Yb:glass laser, we have selected a rod length of 5 mm and a duration of pump pulses of 5 ms as these parameters can provide high gain and uniform distribution.

3. Free-running laser

The experimental setup of the compact free-running Er,Yb:glass laser is shown in figure 3. The laser rod (diameter: 1 mm, length: 5 mm) was prepared from the commercial phosphate glass (LGS-DE synthesized at the Institute of Radio Engineering and Electronics, Russian Academy of Sciences [19], see table 2) doped with the Er^{3+} and Yb^{3+} ions with a concentration of 0.5 × 10^{20} cm^{-3} and 25 × 10^{20} cm^{-3}, respectively. The rod was placed into a ZrO_2 highly efficient diffuse reflector to ensure uniform pump distribution. The rod

Table 1. Parameters of the Er,Yb laser used for the modelling of its performance according to [10].

Parameter[a]	Value
N_{Er}^{0}	5.0×10^{19} cm^{-3}
λ_p	976 nm
λ_L	1535 nm
τ_{Yb}	0.75 ms
τ_{Er}	7.6 ms
α_{ET}	3.7×10^{-16} s^{-1} cm^{-3}
$\sigma_{SE}^{L} \approx \sigma_{abs}^{L}$	0.7×10^{-20} cm^{2}

[a]See explanation in the text.

was passively cooled. The front face of the rod was AR-coated at 976 nm and HR-coated at 1535 nm, so this coating served as a flat pump mirror (PM) of the laser cavity. The rear face of the rod was HR-coated at 976 nm to provide a second pass of the pump beam and AR-coated at 1535 nm. A meniscus output coupler (OC) with the radii of the curvature of both surfaces of $R_{OC} = 32.5$ cm was used. This shape of the OC prevented unwanted defocusing of the output beam.

The rod was pumped through the PM by the unpolarized output of an InGaAs diode bar (ATC—semiconductor devices) emitting up to 16.7 W at 976 nm. The bar was mounted on a Cu-holder and passively-cooled. The diode drive current was electrically modulated to produce a train of rectangular pump pulses with a duration of 5 ms and a repetition frequency of 1 Hz. The emitting area of the bar was 1200×1 μm^2 in size, so the pump beam was reshaped via two fiber lenses AR-coated at 976 nm from both sides. The first lens collimated the pump beam along the 'fast' axis, and the second lens was used as a condenser along the 'slow' axis. As a result, the nearly-circular pump beam with a waist of ~1 mm at the input face of the laser rod was achieved. This design provided a nearly-uniform distribution of the pump radiation in the laser rod and, hence, decreased the temperature and stress gradients under the laser operation.

To optimize the set-up, we varied the total geometrical cavity length L_{cav} and the OC transmission at the laser wavelength T_{OC}. First, L_{cav} was fixed to be 15 mm and several OCs with $T_{OC} = 14\%$, 9.5%, 6% and 3% were studied (figure 4(a)). With the decrease of T_{OC}, the free-running pulse energy E_{out} increased from 3.6–10 mJ (at the maximum pump level, i.e. for the incident pump power energy $E_{inc} = 84$ mJ). Then, we fixed $T_{OC} = 3\%$ and varied the cavity length in the range 10–25 mm (figure 4(b)). For the shortest cavity, E_{out} reached 12 mJ corresponding to a multi-mode laser output. With the increase of the cavity length, the output pulse energy dropped, but for $L_{cav} = 18$ mm, the output laser mode became TEM_{00}. This is explained by the fact that the laser rod acts as an aperture for the laser beam.

Thus, for the further work, $L_{cav} = 18$ mm and $T_{OC} = 3\%$ were selected. In figure 4(c) we plot the free-running output pulse energy E_{out} versus the incident pump pulse energy E_{inc} for this laser configuration. The laser threshold was at E_{inc} ~ 30 mJ and the maximum output energy reached 8.2 mJ corresponding to a slope efficiency of 15% and an optical-to-optical efficiency of ~10%. The duration of laser pulses in the free-running operation mode was ~3 ms.

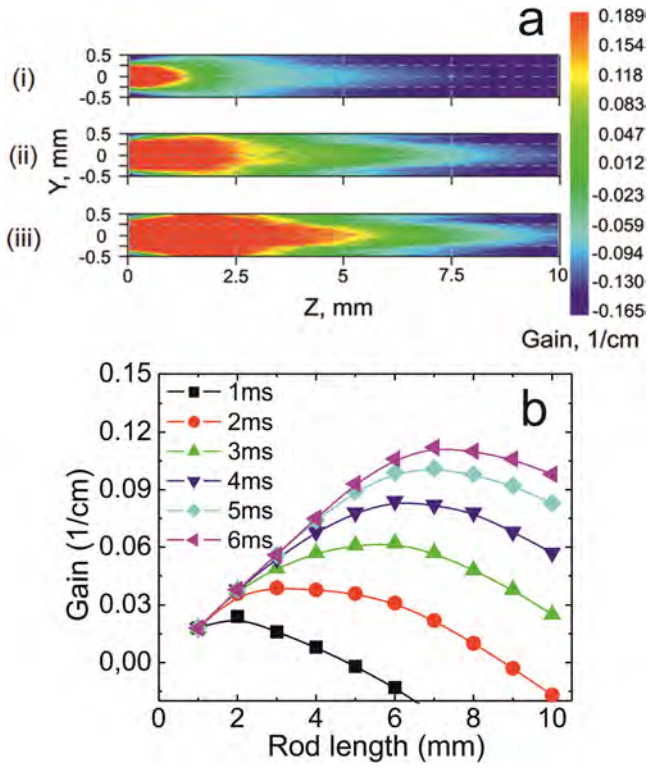

Figure 2. Calculated integral single-pass gain g in a diode-pumped Er, Yb:glass laser rod: (a) spatial distribution of g in the rod cross-section 1 ms (i), 3 ms (ii) or 5 ms (iii) after the pump turn-on. Pump pulses are rectangular with a duration of 5 ms and an energy of 50 mJ; (b) dependence of g versus the rod length at different durations of the pump pulses (1…6 ms).

These parameters are comparable to the best results achieved previously [18]. In [18], a free-running Er,Yb:glass laser was pumped by 10 ms-long pulses at a repetition rate of 2 Hz and the slope efficiency was very similar (15.8%). The maximum pulse energy reached 95 mJ (at $E_{inc} = 720$ mJ) but the laser threshold was three times higher than in our case, at $E_{inc} = 105$ mJ.

The optimized laser was placed in a compact metal housing with dimensions of 15 × 60 mm (figure 3(b)).

4. Passively Q-switched laser

To realize PQS of the designed Er,Yb:glass laser, an SA made of transparent GC was inserted into the laser cavity between the laser rod and OC at the Brewster angle. The cavity with the optimized parameters, $L_{cav} = 18$ mm and $T_{OC} = 3\%$, was used. The temporal profile of Q-switched pulses was detected with a Tektronix TDS2014c digital oscilloscope, and the spatial profile of the laser beam was measured with a CCD-camera.

Two SAs were studied—see inset in figure 5. The first SA was made of GC containing Co^{2+}:$MgAl_2O_4$ (magnesium aluminate spinel) nanocrystals with a mean size of ~10 nm. This GC was developed on the basis of magnesium aluminosilicate glass denoted as MAS doped with 0.03 wt.% CoO and nucleated by a mixture of TiO_2 and ZrO_2 [14]. The second SA was made of GC containing Co^{2+}:γ-Ga_2O_3 nanocrystals with a spinel structure and with the mean size of 8 nm. It was prepared from lithium gallium silicate glass denoted as LGS doped with 0.1 wt.% CoO [16]. The crystallization of both parent glasses

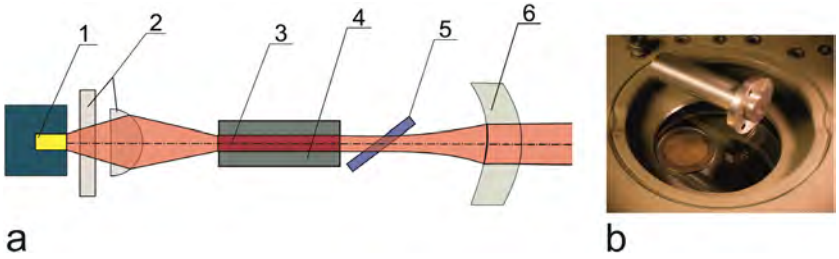

Figure 3. (a) Scheme of the laser set-up: 1—laser diode bar with a heatsink, 2—fiber lenses, 3—laser rod, 4—ZrO_2 diffuse reflector; 5—saturable absorber (for PQS operation), 6—output coupler; (b) photograph of the ready-for-use laser.

Table 2. Physical parameters of the LGS-DE glass[a].

Parameter	Value
Refractive index, n_D	1.53
Thermo-optic coefficient, dn/dT	1.6×10^{-6} K^{-1}
Loss coefficient, δ, at ~1.54 μm	<0.002 cm^{-1}
Thermal expansion coefficient, α	8.0×10^{-6} K^{-1}
Thermal conductivity, κ	0.85 W m^{-1} K^{-1}
Density, ρ	3.0 g cm^{-3}
Knoop hardness	490
LIDT (30 ns-pulses)	>20 J cm^{-2}

[a]Provided by the manufacturer.

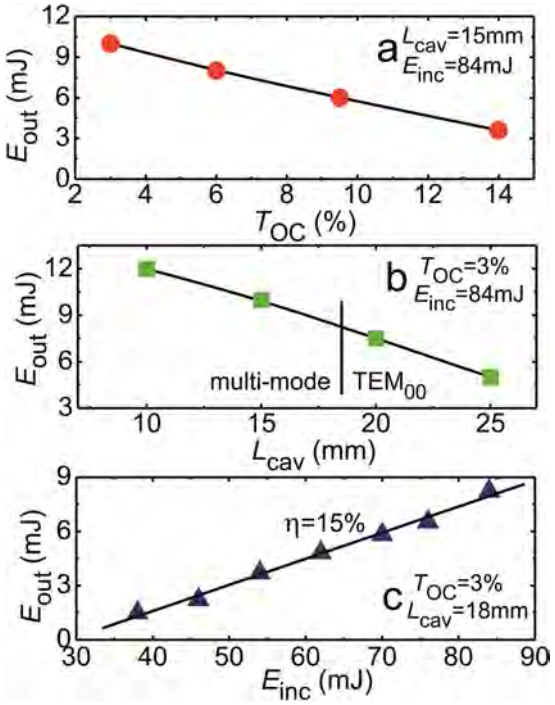

Figure 4. Free-running Er,Yb:glass laser: output pulse energy E_{out} versus the transmission of the output coupler T_{OC} (a) and the total cavity length L_{cav} (b); input–output dependence for the optimal parameters $L_{cav} = 18$ mm and $T_{OC} = 3\%$. η is the slope efficiency.

was ensured by an appropriate heat-treatment performed at a temperature of 950 °C (for Co:MAS) and at 730 °C (for Co:LGS). Both GCs provided a broadband absorption in the range 1.1–1.65 μm (for Co:MAS) and 1.2–1.8 μm (Co:LGS) (see figure 5) related to the $^4A_2(^4F) \rightarrow {}^4T_1(^4F)$ transition of Co^{2+} ions located in the tetrahedral sites of corresponding

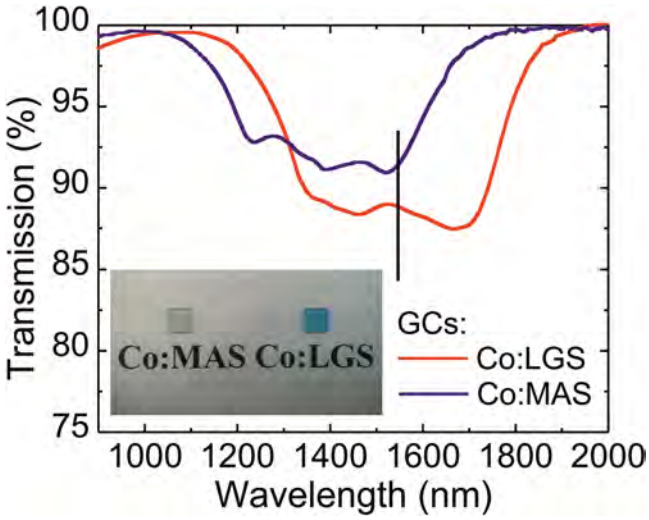

Figure 5. Small-signal transmission of the SAs made of Co:MAS and Co:LGS GCs (SAs: 0.5 mm-thick, oriented at the Brewster angle); the vertical line denotes the laser wavelength. Inset: photographs of the SAs.

Table 3. Parameters of the studied SAs, according to [14, 16].

	Saturable absorber	
Parameter[a]	Co:MAS	Co:LGS
Crystalline phase	Co^{2+}:$MgAl_2O_4$	Co^{2+}:γ-Ga_2O_3
F_S, J cm^{-2}	0.4	0.8
σ_{GSA}, 10^{-19} cm^2	3.2	1.7
σ_{ESA}, 10^{-19} cm^2	0.28	0.2
$\gamma = \sigma_{ESA}/\sigma_{GSA}$	0.088	0.12
τ_{rec}, ns	450	166
δ_{loss}, cm^{-1}	0.04	0.05
t, mm	0.5	0.5
T_{SA}, %	91.5%	87.5%

[a]F_S—saturation intensity, σ_{GSA} and σ_{ESA}—ground- and excited-state absorption cross-section, γ—saturation contrast, τ_{rec}—recovery time of the initial absorption, δ_{loss}—coefficient of passive losses at ~1.54 μm, t—thickness, T_{SA}—small-signal transmission at the Brewster angle.

nanocrystals. The scheme of the energy-levels of the Co^{2+} ions is shown in figure 1(b).

Nonlinear properties of these GCs, namely the saturation fluence $F_S = h\nu_L/\sigma_{GSA}$, the ground- and excited-state absorption cross-sections σ_{GSA} and σ_{ESA} of the Co^{2+} ions, respectively, and the recovery time of the initial absorption τ_{rec}, are presented in table 3. Both SAs with a thickness of 0.5 mm were polished to

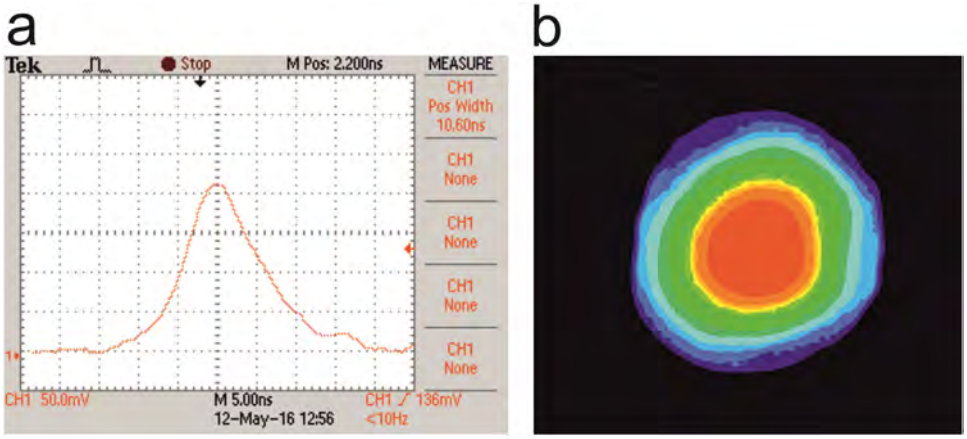

Figure 6. Passively Q-switched Er,Yb:glass laser: (a) oscilloscope trace of a single Q-switched pulse; (b) spatial profile of the laser beam for the SA based on the Co:MAS GC.

laser quality from both sides and remained uncoated. The initial (small-signal) transmission of the SAs, T_{SA}, determined for the Brewster angle orientation was 91.5% (Co:MAS) and 87.5% (Co:LGS) at the laser wavelength of 1.54 μm.

Co^{2+}-doped SAs for Er lasers can be considered as the 'slow' ones, as the characteristic recovery time of the initial absorption τ_{rec} (few hundreds of ns) is much longer than the time of a single Q-switched pulse formation (a few tens of ns). There is the criterion for efficient PQS with a 'slow' SA [20]:

$$X = \frac{S_{AE}}{S_{SA}} \frac{\sigma_{SA}^{eff}}{\sigma_{SE}^{L} + \sigma_{abs}^{L}} \gg 1, \quad (3)$$

where $\sigma_{SA}^{eff} = \sigma_{GSA} - \sigma_{ESA}$ is the effective absorption cross-section of the SA, S_{AE} and S_{SA} are the mode areas in the active element and SA, respectively (in the latter case one needs to take into account the Brewster-angle orientation of the SA). According to the ABCD modelling of the designed cavity, $S_{AE} \approx S_{SA}$. Using the spectroscopic parameters listed in tables 1 and 2, we calculated $X = 21$ and 11 for SAs based on GCs with the Co^{2+}:$MgAl_2O_4$ and Co^{2+}:γ-Ga_2O_3 nanocrystals, respectively, which proves the possibility of efficient PQS of the designed laser.

When using SA made of Co:MAS GC, the developed laser generated stable pulses with the energy of $E_{out} = 0.7$ mJ and the duration of $\Delta\tau = 10.5$ ns (full width at half maximum, FWHM). The oscilloscope trace of a single Q-switched pulse is shown in figure 6(a). Thus, the peak power reached $P_{peak} = E_{out}/\Delta\tau = 67$ kW. The conversion efficiency with respect to the free-running operation mode η_{conv} was 9%. The laser generated a nearly-circular output beam (figure 6(b)), with a measured divergence of 5.3 mrad corresponding to a beam quality factor $M^2 = 1.4$. For the SA made of Co:LGS GC, the pulse characteristics were 0.5 mJ/11 ns, $P_{peak} = 45$ kW and $\eta_{conv} = 6\%$.

During the long-term operation of the passively Q-switched Er,Yb:glass laser, no signs of laser damage to the SA were detected. One can estimate the intracavity fluence on the SA as [20]:

$$F_{in} = \frac{2 - T_{OC}}{T_{OC}} \frac{2E_{out}}{S_{SA}}. \quad (4)$$

Here, we again consider the Brewster-angle orientation of the SAs. For SAs made of Co:MAS and Co:LGS GCs, $F_{in} = 6.4$ J cm^{-2} and 4.6 J cm^{-2}, respectively. These values are well below the LIDT for uncoated and laser quality-polished GCs (~10 J cm^{-2}, as measured at ~1.54 μm for ns-long pulses).

5. Discussion

Recently, GCs containing various Co^{2+}-doped nanocrystals have been employed for PQS of Er,Yb:glass lasers with a diode-side-pumping operating at the repetition frequency of 1 Hz. In table 4, we have compared the output characteristics of these lasers and the developed oscillator. The designed laser provides a short pulse duration and high peak power, as well as a high Q-switching conversion efficiency, as compared with the previous results.

Further shortening of the pulses in PQS Er,Yb:glass lasers can be reached by using the microchip laser concept [2, 22, 23], with the active element and SA both placed in a compact plano–plano laser cavity and the laser mirrors directly deposited on their surfaces. Pulse shortening down to a few ns may occur due to the reduction of the cavity roundtrip time [22]. There are several requirements for SAs used in monolithic microchip lasers. Such SAs should provide: (i) low absorption of residual pump light to prevent the SA heating and, hence, Q-switching instabilities, (ii) relatively high LIDT, as the size of the laser mode in microchip lasers (which is determined by the thermal lens of the active element) is relatively small and the intracavity fluence is high [24], (iii) similar thermal expansion to the laser element to avoid thermal fracture. The developed GCs seem to be very promising for this aim, as the absorption bands of the Co^{2+} ions do not overlap with the pump wavelength (see figure 5), LIDT is relatively high (see above) and the thermal expansion coefficient is low, namely $\alpha = 4.9 \times 10^{-6}$ K^{-1} (for Co:MAS), and is comparable to that of the Er,Yb:glass (see table 2).

Due to the broadband absorption of Co^{2+} ions in the Co:LGS GCs (see figure 5) one may potentially use it for PQS of crystalline Er lasers emitting at 1.6–1.7 μm (e.g. Er:YAG laser) or even thulium (Tm) lasers emitting in the

Table 4. Comparison of the output characteristics[a] of passively-cooled Er,Yb: glass lasers passively Q-switched with GC SAs reported so far.

Crystalline phase in GCs	E_{out}, mJ	$\Delta\tau$, ns	P_{peak}, kW	η_{conv}, %	Ref.
Side-pumping					
Co^{2+}:γ-Ga_2O_3	1.75	25	70	10	[16]
Co^{2+}:ZnO	0.37	100	3.7	2.2	[17]
Co^{2+}:Zn_2SiO_4	0.77	45	17	2.7	[21]
End-pumping					
Co^{2+}:$MgAl_2O_4$	0.7	10.5	66	9	This work
Co^{2+}:γ-Ga_2O_3	0.5	11	45	6	This work

[a] E_{out}—pulse energy, $\Delta\tau$—pulse duration (FWHM), P_{peak}—peak power, η_{conv}—Q-switching conversion efficiency.

eye-safe spectral range 1.8–1.9 μm. The application of Co^{2+}-doped materials for PQS of Tm lasers is known [25]. However, in this case, the laser wavelength will correspond to the edge of the absorption band resulting in lower σ_{GSA}. This will have two consequences. First, to reach the required modulation depth of the SA, one needs to increase the CoO concentration up to 0.5–1.0 wt.%. Second, lower σ_{GSA} means higher F_S, so it is more difficult to achieve bleaching of the SA. For Co:LGS GCs at ~1.85 μm, we estimate σ_{GSA} as ~0.2×10^{-19} cm^2. This is lower than for the state-of-the-art SA for this spectral range, Cr^{2+}:ZnS, for which $\sigma_{GSA} = 6.7 \times 10^{-19}$ cm^2 [24]. However, GCs may offer much better optical quality and higher LIDT as compared to polycrystalline Cr^{2+}:ZnS.

Transparent polycrystalline Co^{2+}-doped ceramics, e.g. based on $MgAl_2O_4$, may be considered as alternative materials for transparent GCs. However, such ceramics typically suffer from very low LIDT, ~3 J cm^{-2}, high scattering losses and degradation of optical properties with the increase of Co^{2+} concentration [26].

6. Conclusion

We have developed a compact and robust eye-safe (~1.54 μm) passively-cooled Er laser. The laser head is 15 × 60 mm in size and its average electric power consumption is 0.18 W. In the free-running regime, the laser-generated 8.2 mJ pulses correspond to a slope efficiency of 15%. The PQS of this laser is provided by two SAs made of transparent GCs containing Co^{2+}:γ-Ga_2O_3 and Co^{2+}:$MgAl_2O_4$ spinel nanocrystals. The passively Q-switched Er,Yb:glass laser generated 0.7 mJ/10.5 ns and 0.5 mJ/11 ns pulses (for these two SAs, respectively) at a repetition frequency of 1 Hz. The output beam of the laser corresponded to the TEM_{00} mode ($M^2 = 1.4$) with a divergence of 5.3 mrad. The designed laser head is promising for range-finding systems.

Acknowledgments

V V Vitkin, A A Zhilin and O S Dymshits express their gratitude to the RFBR (Grant 16-03-01130) for partial support of this work.

References

[1] ANSI Standard Z136.1 2007 *American National Standard for Safe Use of Lasers*
[2] Mlynczak J and Belghachem N 2015 *Opt. Commun.* **356** 166–9
[3] Mak A A, Polyakov V M, Vitkin V V, Kharitonov A A, Buchenkov V A, Rodionov A Y, Alekseeva A P, Dymshits O S and Zhilin A A 2015 *Proc. SPIE* **9342** 93421K
[4] Sulc J, Jelınkova H, Ryba-Romanowski W and Lukasiewicz T 2009 *Laser Phys. Lett.* **6** 207–11
[5] Jiang D P, Zou Y Q, Su L B, Tang H L, Wu F, Zheng L H, Li H J and Xu J A 2011 *Laser Phys. Lett.* **8** 343–8
[6] Zendzian W, Gałecki L, Jabczynski J K, Kwiatkowski J, Gorajek L, Nemec M, Jelinkova H and Sulc J 2010 *Laser Phys.* **20** 470–3
[7] Wan P and Liu J 2012 *Proc. SPIE* **8235** 82351Y
[8] Nettleton J E, Schilling B W, Barr D N and Lei J S 2000 *Appl. Opt.* **39** 2428–32
[9] Park D-H, Jeon H-H and Oh S-I 2007 *Chin. Opt. Lett.* **5** S243–5
[10] Boutchenkov V, Kuchma I, Levoshkin A, Mak A, Petrov A and Hollemann G 2000 *Opt. Commun.* **177** 383–8
[11] Karlsson G, Laurell F, Tellefsen J, Denker B, Galagan B, Osiko V and Sverchkov S 2002 *Appl. Phys.* B **75** 41–6
[12] Jiang S, Myers M and Peyghambarian N 1998 *J. Non-Cryst. Solids* **239** 143–8
[13] Yumashev K V, Denisov I A, Posnov N N, Prokoshin P V and Mikhailov V P 2000 *Appl. Phys.* B **70** 179–84
[14] Volk Yu V, Denisov I A, Malyarevich A M, Yumashev K V, Dymshits O S, Shashkin A V, Zhilin A A, Kang U and Lee K-H 2004 *Appl. Opt.* **43** 682–7
[15] Denisov I A, Volk Yu V, Malyarevich A M, Yumashev K V, Dymshits O S, Zhilin A A, Kang U and Lee K-H 2003 *J. Appl. Phys.* **93** 3827–31
[16] Loiko P A *et al* 2015 *Laser Phys. Lett.* **12** 035803
[17] Loiko P A *et al* 2016 *Laser Phys. Lett.* **13** 055803
[18] Tanguy E, Feugnet G, Pocholle J P, Blondeau R, Poisson M A and Duchemin J P 1998 *Opt. Commun.* **145** 105–8
[19] Byshevskaya-Konopko L O, Vorob'ev I L, Izyneev A A and Sadovski P I 2004 *Quantum Electron.* **34** 809–11
[20] Siegman A E 1986 *Lasers* (Mill Valley, CA: University Science Books)
[21] Loiko P A *et al* 2016 *Appl. Opt.* **55** 5505–12
[22] Häring R, Paschotta R, Fluck R, Gini E, Melchior H and Keller U 2001 *J. Opt. Soc. Am.* B **18** 1805–12
[23] Kisel V E, Gorbachenya K N, Yasukevich A S, Ivashko A M, Kuleshov N V, Maltsev V V and Leonyuk N I 2012 *Opt. Lett.* **37** 2745–7
[24] Loiko P, Serres J M, Mateos X, Yumashev K, Yasukevich A, Petrov V, Griebner U, Aguiló M and Díaz F 2015 *Opt. Lett.* **40** 5220–3
[25] Hecht H, Katzir A, Burshtein Z, Sokol M, Noach S, Frumker E, Galun E and Ishaaya A A 2006 *Europhoton-2016 (Vienna, 21–26 August 2016)* (European Physical Society) P. PO-3.26
[26] Goldstein A, Loiko P, Burshtein Z, Skoptsov N, Glazunov I, Galun E, Kuleshov N and Yumashev K 2016 *J. Am. Ceram. Soc.* **99** 1324–31